Assessment of Seismic Demands caused by 12 November 2017 Ezgeleh Earthquake (Mw=7.3) in Kermanshah

B. Ghanbari[1*] and A.H. Akhaveissy[2]

[1] Ministry of Roads & Urban Development, Kermanshah, Iran
[2]Department of Civil Engineering, Razi University, Kermanshah, Iran

ABSTRACT: A severe earthquake ground motion with a moment magnitude of Mw=7.3 took place in the western part of Iran on 12 November 2017. The main objective of this study is to evaluate the seismic demands of structures under the recent November 12, 2017, Ezgeleh (Mw=7.3) earthquake. For this purpose, we selected the ground motions recorded at Sarpol-e-Zahab, Goorsefid, Kerend, and Javanrood stations that have maximum PGA. Evaluation is conducted by generalized inter-story drift spectra, input energy spectra and ductility demands (μ) computed for selected records. Also, the time evolution of the frequency-intensity content of selected records is discussed based on the Wavelet Transform (WT). Results showed that the (E-W) components trigger larger inter-story drift demands than those from the (N-S) components. Particularly, it was identified that Sarpol-e Zahab and Goorsefid stations produced inter-story drift demands significantly larger than those at other recording stations. Time-frequency analysis of ground-motions recorded at the Sarpol-e Zahab station shows that there is a transition of energy content of E-W component with lower periods (i.e. 0.25 sec) to moderate periods (i.e.0.50,0.75 sec) that it has a potential for moving resonance in buildings with short periods between (0.2-0.5 sec). Also, it can be observed that most energies of the N-S component were highly concentrated at a long period band (between 0.9 and 1.5 sec) that is considered as pulse-like. These findings are consistent with the damage observed in Sarpol-e-Zahab and its villages, where many dwellings and buildings collapsed or suffered severe damage during this event have a low fundamental period between)0.2 and 0.5 sec).

1. INTRODUCTION

A strong earthquake with Mw=7.3 occurred on the western part of Iran at 21:48 and 18:18 UTC of 12 November 2017. The epicenter of this shock has a distance of about 5 km to the town of Ezgeleh, 43 km from Sarapul-e Zahab city, and 46 km from Qasr-e-Shirin city. This event that continued for 30 sec was felt in an extended area in Iran, Mesopotamia, the Caucasus, eastern Turkey, Iraq, and Syria. Until 22 March 2018, about 700 aftershocks with magnitudes over 2.5 have been recorded by the Iranian Seismological Center (IRSC). The largest magnitude of this earthquake's aftershock sequence was 4.8, which occurred on 13 November 2017. During this earthquake (Mw = 7.3), many villages were completely destroyed and different damage levels were observed in the cities of Sarpol-e Zahab, Qasr-e Shirin, and Islamabad-e Gharb. Reports show that more than 600 people were killed, at least 12,000 were injured, more than 30,000 were left homeless, and widespread damage was caused to the buildings [1]. The most collapsed buildings are observed in Sarpole-Zahab (Fig. 1).

This technical note primarily purposed to investigate seismic demands triggered in the Kermanshah city from the recent 12 November 2017 (Mw=7.3) Ezgeleh earthquake. The generalized inter-story drift spectra, inelastic input energy spectra, and ductility demand spectra computed in this regard for selected recording stations in various soil sites of Kermanshah city are provided. The chosen recording stations involve the heavily destroyed areas of the city. Also, the time evolution of the energy and frequency-intensity content of selected records are discussed based on the Wavelet Transform (WT) methodology.

2. GROUND MOTION RECORDS

Ground motions during the 2017 Sarpol-e Zahab earthquake were recorded at 109 stations of Iran Strong-Motion Network (ISMN) [2]. Uncorrected strong motion data were processed to make baseline and then filtered with a fourth-order Butterworth bandpass filter in the frequency range of 0.1-25Hz. In this study, the data recorded at four stations with top PGA values were put in the analysis with more detail. Table 1 lists the main characteristics of the selected records in horizontal components. The Sarpol-e Zahab city has experienced a higher value of peak ground acceleration, velocity, and displacement in the study region as 0.686 g, 52.79 cm/s, and 30.45 cm, respectively. Fig. 2 shows

*Corresponding author's email: bakhtiyar.ghanbari@yahoo.com

Fig. 1. Collapsed building in Sarpol-e Zahab city.

Table 1. Ground motion parameters at the four selected stations.

Station name	Comp.	PGA (cm/s/s)	PGV (cm/s)	Epi distance (km)	Soil type
Sarpol_e Zahab	E-W	563.37	52.79	39.1	II
Sarpol-e Zahab	N-S	686.47	45.55	39.1	II
Goorsefid	E-W	239.65	28.19	66.1	II
Goorsefid	N-S	280.70	23.67	66.1	II
Kerend	E-W	283.49	37.30	66.2	I
Kerend	N-S	204.36	25.14	66.2	I
Javanrood	E-W	178.37	18.44	53	III
Javanrood	N-S	231.08	25.05	53	III
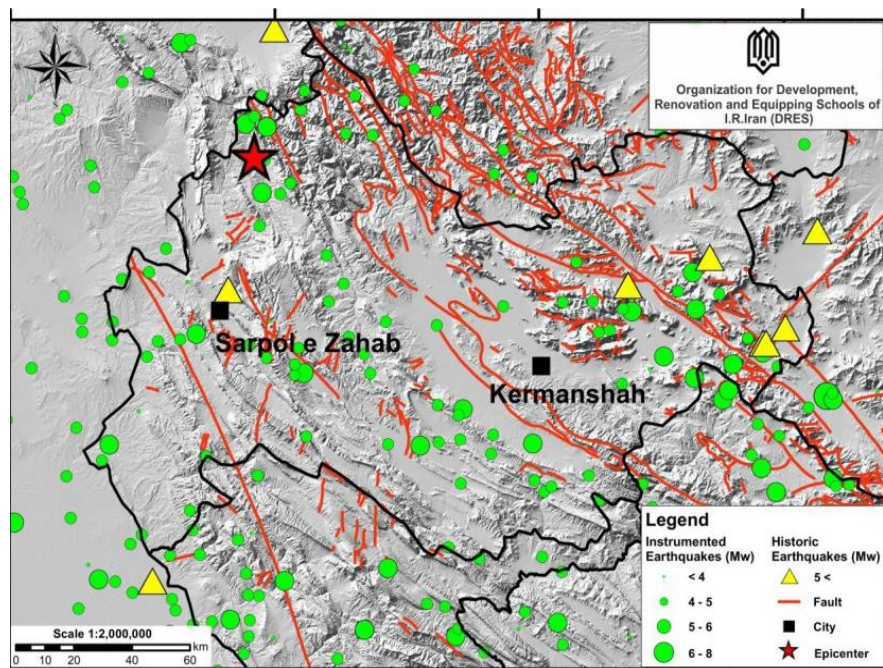
Fig. 2. Seismicity of the region ((reconstructed from preliminary report on school buildings performance of Organization for Development, Renovation and Equipping Schools of I.R. Iran, 2017[3])

the seismicity of the region.

3. TIME-FREQUENCY ANALYSIS OF GROUND MOTION RECORDS

The structural damage has a direct relationship with important parameters of the ground motion such as frequency content, significant duration, and amplitude. Unlike the amplitude and significant duration parameters, the frequency content is not estimable from the ground motion time history. Rather, this information is hidden behind the ground motion record that various mathematical tools are required for its extraction. To analyze the time-varying frequency content of ground motions, several tools were developed, including the Wavelet Transform (WT), the Short Time Fourier Transform (STFT), and the Wigner-Ville Distribution (WVD) [4-6]. WT is a powerful tool for time-frequency analysis and has a good time-frequency discrimination ability. Subsequently, several researchers have applied a wavelet transform to time-frequency analysis of earthquake strong motion [7-11]. In general, the WT of the signal, *x(t)*, is defined as a following inner product:

$$C(a,b) = \int_{-\infty}^{+\infty} f(t) \psi_{a,b}(t) \tag{1}$$

Where $\psi a,b(t)$ is the mother wavelet function and is defined as:

$$\psi_{a,b}(t) = \frac{1}{\sqrt{s}} \psi\left(\frac{t-b}{a}\right) \tag{2}$$

Where *a* is scale variable, *b* is shift in time. In this paper, complex morlet wavelet has been chosen as mother wavelet in the analysis. The complex morlet mother wavelet is suiTable for the analysis spectral nonstationarity of ground motion acceleration time histories [12]. The complex morlet wavelet function is shown in Fig. 3.

The aim of this section is to investigate the time evolution of the energy and frequency content of ground motions recorded using the WT methodology. For this purpose, the implementation of WT is done by first discretizing the ground motion in time and then sampling it with translation parameters *b* at scale parameters *a* to achieve an appropriate frequency resolution. The relationship between scale, *a*, and frequency can be explained by the pseudo period corresponding to each scale. The pseudo-period corresponding to each scale as follow:

$$T_a = \frac{a \times \Delta}{f_c} \tag{3}$$

Where *α* is a scale, Δ is the sampling period, *fc* is the central frequency of a wavelet used in the analysis in Hz. The wavelet map is created using a continuous wavelet transform with the complex Morlet wavelet and shows the variation of
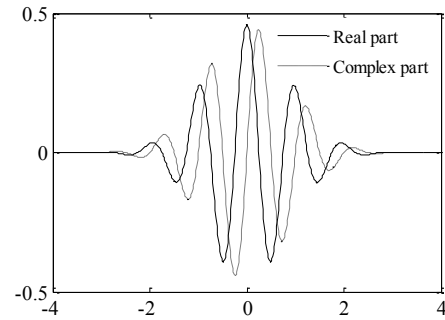
Fig. 3. Complex Morlet wavelet
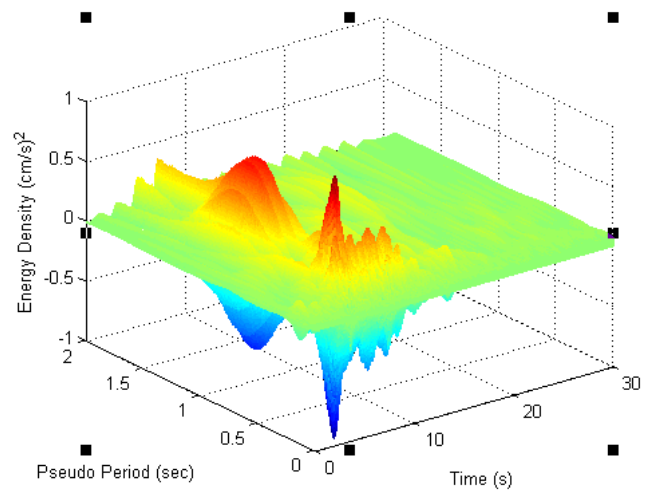
Fig. 4. Three-dimensional wavelet map or time-frequency-amplitude distribution for the N-S component of ground motion recorded at sarpol-e Zahab station

ground motion energy against time. Three dimensional time-frequency energy density distribution for the N-S component of Sarpol-e-Zahab record with WT is shown in Fig. 4. Also, Fig. 5 presents the Two-dimensional wavelet map of the N-S component of Sarpol-e-Zahab record. Regarding the acceleration time history of N-S component, it can be seen that the ground motion energy is concentrated in the initial portions of the record (between 4 and 8 sec from initiating the record). Also, the ground motion had two distinct ridges of energy in which the second has a longer period than the first, but a smaller intensity. The strong burst of energy in low periods is extremely concentrated in a short length of the period (between 0.2 and 0.3 sec) at the time (at about 4 sec in the time scale). Also, it can be observed that the energy of higher period energy ridge is concentrated in time about 5-7 sec (in the time scale) but is distributed over a wide range of periods that starts at a predominant period of 0.9 sec and shifts to strong frequency content at a period of about 1.5 sec that is considered as pulse-like. Therefore, the wavelet map in Fig. 5 reveals a pulse at periods of about 1.2 sec. Based on the results of past studies, records characterized by directivity concentrate most of the energy in a few pulses at the initial portions of the record [13]. Evidently, the particular
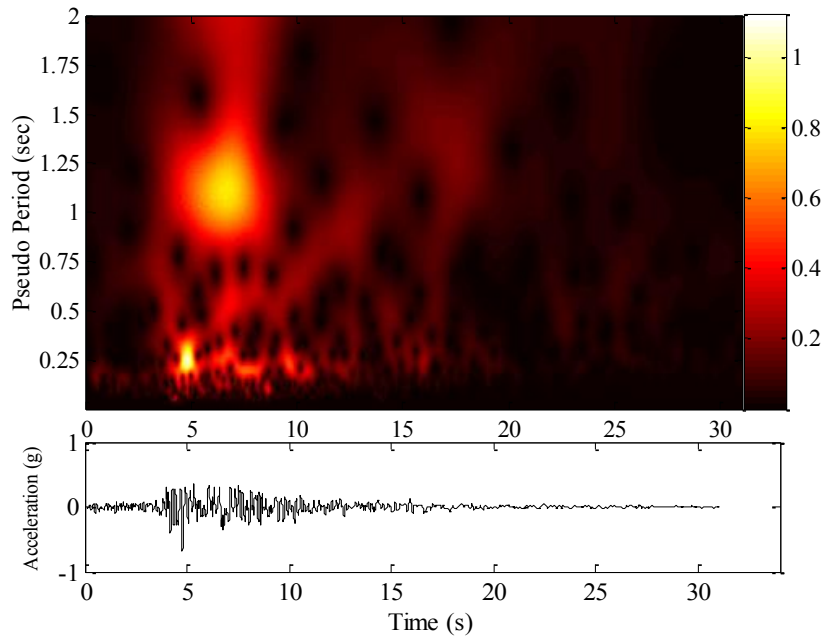
Fig. 5. Two-dimensional Wavelet map for acceleration the N-S component of ground motion recorded at sarpol-e Zahab station.
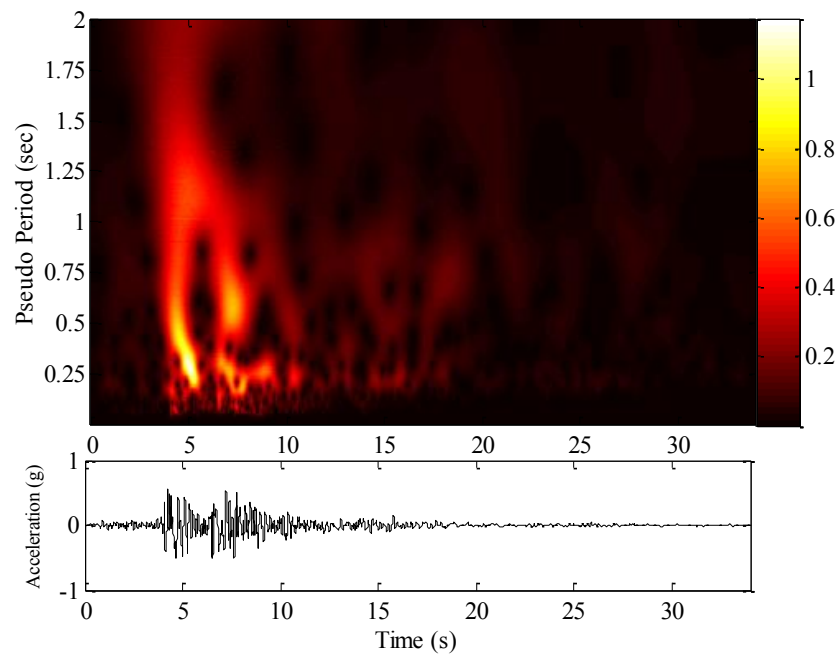
Fig.6. Two-dimensional Wavelet map for acceleration the E-W component of ground motion recorded at sarpol-e Zahab station.

dominant periods of this component and their evolution in time recognized 'directivity' effect. Fig. 6 shows the Two-dimensional wavelet map for E-W component recorded at Sarpol-e Zahab station. As can be clearly seen, an energy transition with a significant portion exists that starts with very low periods (i.e. 0.2 sec) and shifts to short periods (i.e.0.50 sec) in a narrow time band (i.e., 3-5 sec). The second dominant ridge of energy with smaller intensity is at periods around 0.6 sec. It is expected that this trend in the ground motion has been conducive to moving resonance on buildings with low periods between (0.2-0.5 sec). This means that structures with

shorter periods, in coincidence with a first dominant ridge of energy in the record, may be subjected to significant damage and their fundamental period increases while the second dominant ridge of energy reaches the structure.

According to these findings, the concentrated energy of records in time and frequency resulted in an increase in damage at the surrounding area of Sarpol-e Zahab city, which was the worst affected area. It is also possible to note that for two components, the strong component of the record at a low period band was highly concentrated in the initial portions of the record. This result is consistent with the
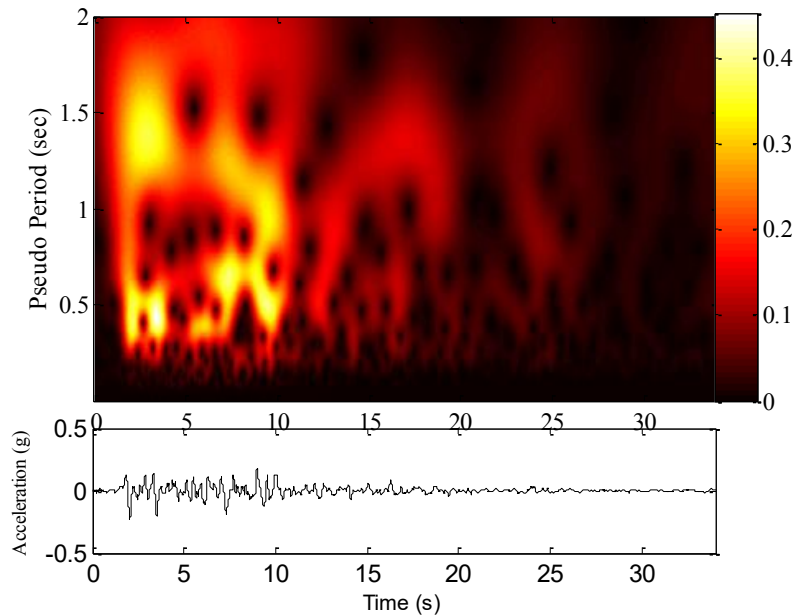
Fig. 7. Two-dimensional Wavelet map for acceleration the E-W component of ground motion recorded at Javanrood station.
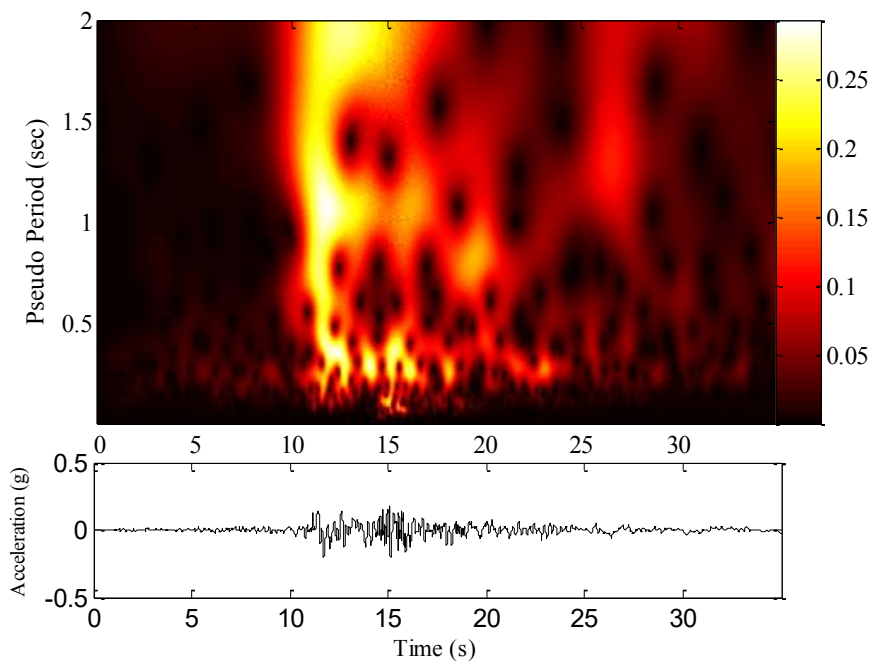
Fig. 8. Two-dimensional Wavelet map for acceleration the N-S component of ground motion recorded at Kerend station.

damage level found in Sarpol-e-Zahab and its villages, where a low fundamental period (i.e., 0.2-0.5 sec) existed for many dwellings and buildings collapsed or suffered severe damage during this occurrence. All these results are consistent with the findings of Yaghmaei-Sabegh [14].

Fig. 7 illustrates the Two-dimensional wavelet map and acceleration time history for the Javanrood record. The seismogram was recorded at the Javanrood station during the Ezgalah earthquake. This station is located on the type-C site. Fig. 7 demonstrates that the significantly high energy content of E-W component of Javanrood record concentrated

at the beginning of the record (i.e., 2-10 sec of the record). Also, this ground motion has a high energy at several periods, which have high peaks for a long period of time. The E-W component of Javanrood is a ground motion with long-period components. Another interesting point that can be noticed by the use of the WT, which was not possible to observe in the time or frequency domains separately, is that the wavelet map explicitly demonstrates how the period of the motion gradually increases from period content 0.3 to 2 sec, which suggests soil softening. During severe earthquake shocks, soil softening leads to period elongation of the site fundamental

period and soft-soil records convey a period content below 2 sec [15, 16]. Therefore, it is expected that this trend in the ground motion has led to the resonance of the buildings with long fundamental periods. Large long-period components are common in records with directivity effect, surface waves, and/ or site amplification [17]. Fig. 8 shows the Two-dimensional wavelet map and the time history acceleration of the N-S component of Kerend record that was recorded on very hard soil (Type 1). It is clear from this wavelet map that the strong long-period component of the Kerend record is present in the middle portions of the record (between 10 and 15 s from the beginning of the record). This wave trend in which strong longer period components arrive later in the acceleration time history is caused by the slower traveling long period surface waves.

4. GENERALIZED INTER-STORY DRIFT SPECTRA

Inter-story Drift Ratio (IDR) is one of the particularly useful engineering response quantity and indicator of structural performance, especially for high-rise buildings [18-20]. Miranda and Akkar [21] used the Csonka's [22] flexural-shear beam model, shown in Fig. 9, to obtain estimates of drift demands in linearly elastic multi-story buildings. The flexural and shear beams are assumed to be connected by an infinite number of axially rigid members, which are pinned at their ends, transmitting horizontal forces only so that the flexural beam and the shear beam undergo the same lateral movements. Mass and stiffness are assumed to be uniformly distributed and constant along building height. When the flexural-shear beam model is subjected to an acceleration time history $\ddot{u}_g(t)$, the inter-story drift ratio at the jth story is estimated by [21]:

$$IDR(j,t) \approx \frac{1}{H} \sum_{i=1}^{m} \Gamma_i \phi_i'(x) D_i(t), \qquad (4)$$

Where H is the height of the building, Γ_i is the modal participation factor associated with the ith mode, and $\phi_i'(x)$ is the first derivative of the ith mode at a non-dimensional height x of the beam model which is the average height of the j + 1 and j floors. Also, $D_i(t)$ is the displacement response of a damped SDOF system with elstic period T_i and modal damping ratio corresponding to those of the ith mode of vibration. The simplified building model can be defined by their fundamental period T, modal damping ratio ξ and the lateral dimensionless stiffness ratio, α, expressed as function of the ratio of shear to flexural rigidities as follows:

$$\alpha = H \sqrt{\frac{GA}{EI}} \qquad (5)$$

H is the height of the building, GA is the shear rigidity of the shear beam and EI is the flexural rigidity of the flexural beam. Setting α=zero the model corresponds to a Bernoulli beam (pure flexural model) while setting α = 650 the model
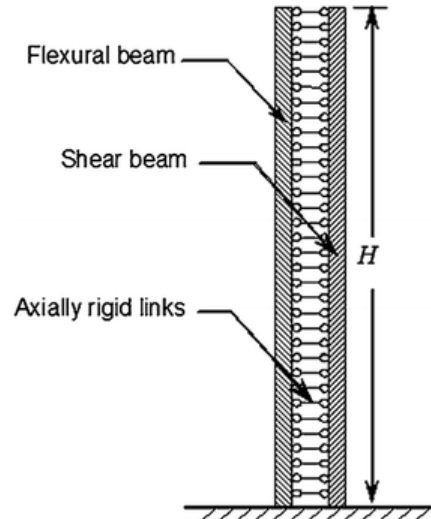
Fig. 9. Simplified model for assessing building response (Miranda and Akkar [14]).

corresponds to a shear beam (pure shear model). Some research used this simplified model to estimate maximum inter-story drift ratio IDR_{max} in multi-story buildings when subjected to pulse-like ground motions [23-27].

IDR_{max} for each record computed for Bernoulli beam (α= 0.01) and shear beams (α= 650) with 5% damping ratio and with elastic periods between 0.05 and 5.0 sec is presented in Figs. 10 and 11. Generally, it can be observed that the E-W components trigger larger IDR_{max} demands compared to the N-S components. Particularly, the N-S component of Sarpol-e Zahab and E-W component of Goorsefid stations produced significantly larger IDR_{max} demands in excess of 1.5% than other stations.

The inter-story drift spectra of N-S component of Sarpol-e Zahab station indicate a clear amplification in the period around 1.2 sec. The pulse caused by directivity effect may be the reason for this amplification.

There is also a small difference between the results of low lateral stiffness ratio systems (i.e., 0.01) and the high level lateral stiffness ratio systems (i.e., 650). These phenomena indicate that the buildings with high lateral stiffness ratio involve larger IDR_{max}.

By employing a bilinear hysteretic model, this study investigates the input energy and ductility demands of structures subjected to selected ground motions. Based on the numerical results, some insights into the effect of Sarpol-e Zahab ground motions excitations on structures are presented.

5. STRUCTURAL MODEL

This paper examines bilinear SDOF systems under selected ground motions. The equation of motion bilinear SDOF systems with linear hardening under earthquake excitation is given by:

$$m\ddot{u} + c\dot{u} + f_s = -m\ddot{u}_g \qquad (6)$$
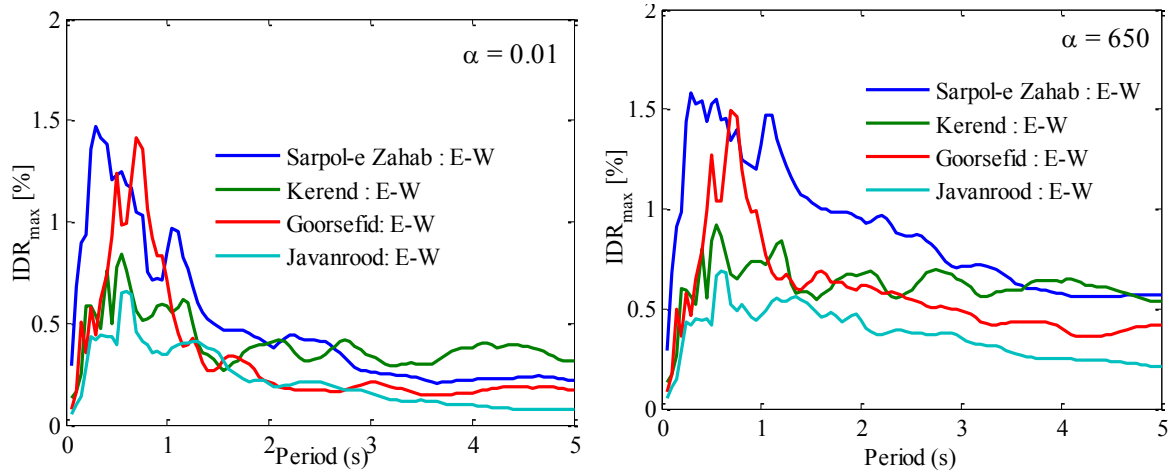
Fig. 10. Inter-story drift spectra computed for E-W component of selected records: a) α= 0.01 b) α= 650
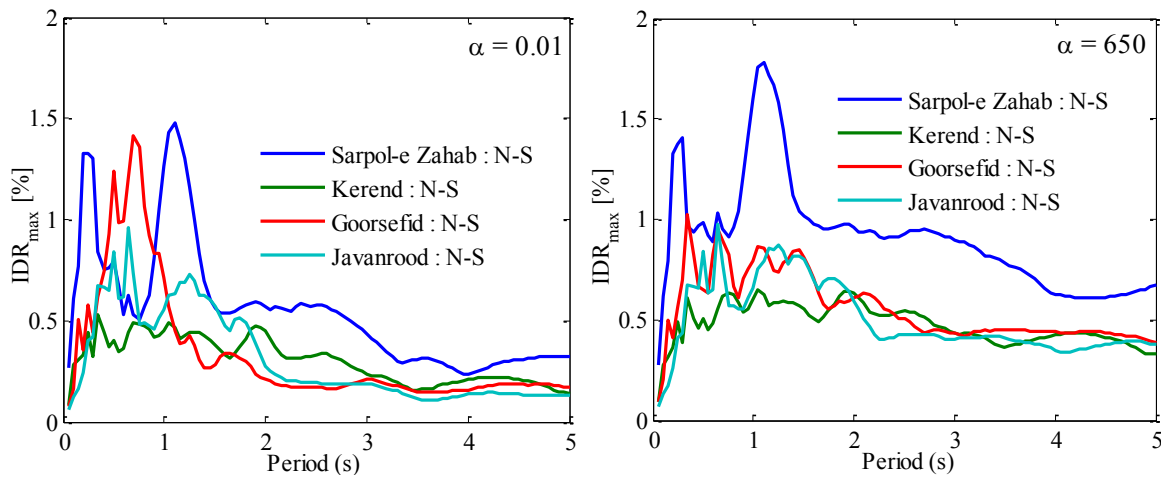
Fig. 11. Inter-story drift spectra computed for N-S component of selected records: a) α= 0.01 b) α= 650.

Where m is mass of the system; c is damping coefficient; fs is restoring force; $\ddot{u}g$ is ground acceleration; and $\ddot{u}$, $\dot{u}$, and u are the relative acceleration, velocity, and displacement of the system with respect to the ground, respectively[28]. The present study evaluated inelastic SDOF systems with a period range of 0.1 s–5.0 s with a time-step of 0.1 s. In this study, seismic ductility demand was chosen as the parameter representative of damage due to large deformations. The relative lateral strength is measured by the lateral strength ratio R, which is defined as:

$$R = \frac{F_e}{F_y} \qquad (7)$$

Where F_e is the strength demand on an infinitely elastic SDOF system during the prescribed earthquake excitation, and F_y is the yielding strength of the corresponding inelastic SDOF system with the same mass and initial stiffness. Four values of R were considered (i.e., R = 1, 2, 4, and 6) to examine the influence of structural strength. A typical force–displacement response of SDOF bilinear model under seismic
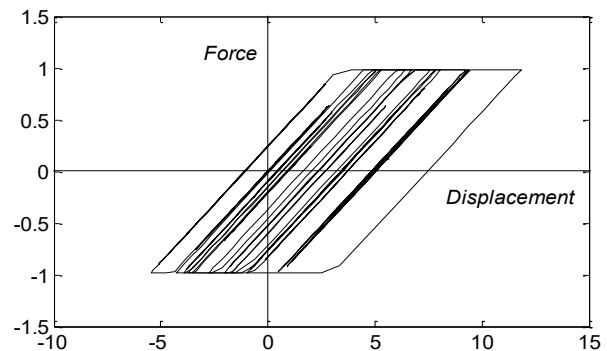
Figure 12. Force–displacement response of elastic-perfectly plastic SDOF

loading is shown in Fig. 12.

6. ELASTIC AND INELASTIC INPUT ENERGY

More recently, the input energy of earthquake excitation has been widely recognized as one of the key factors related to the structural damage. Accordingly, more rational seismic design methods based on energy criterions incorporating
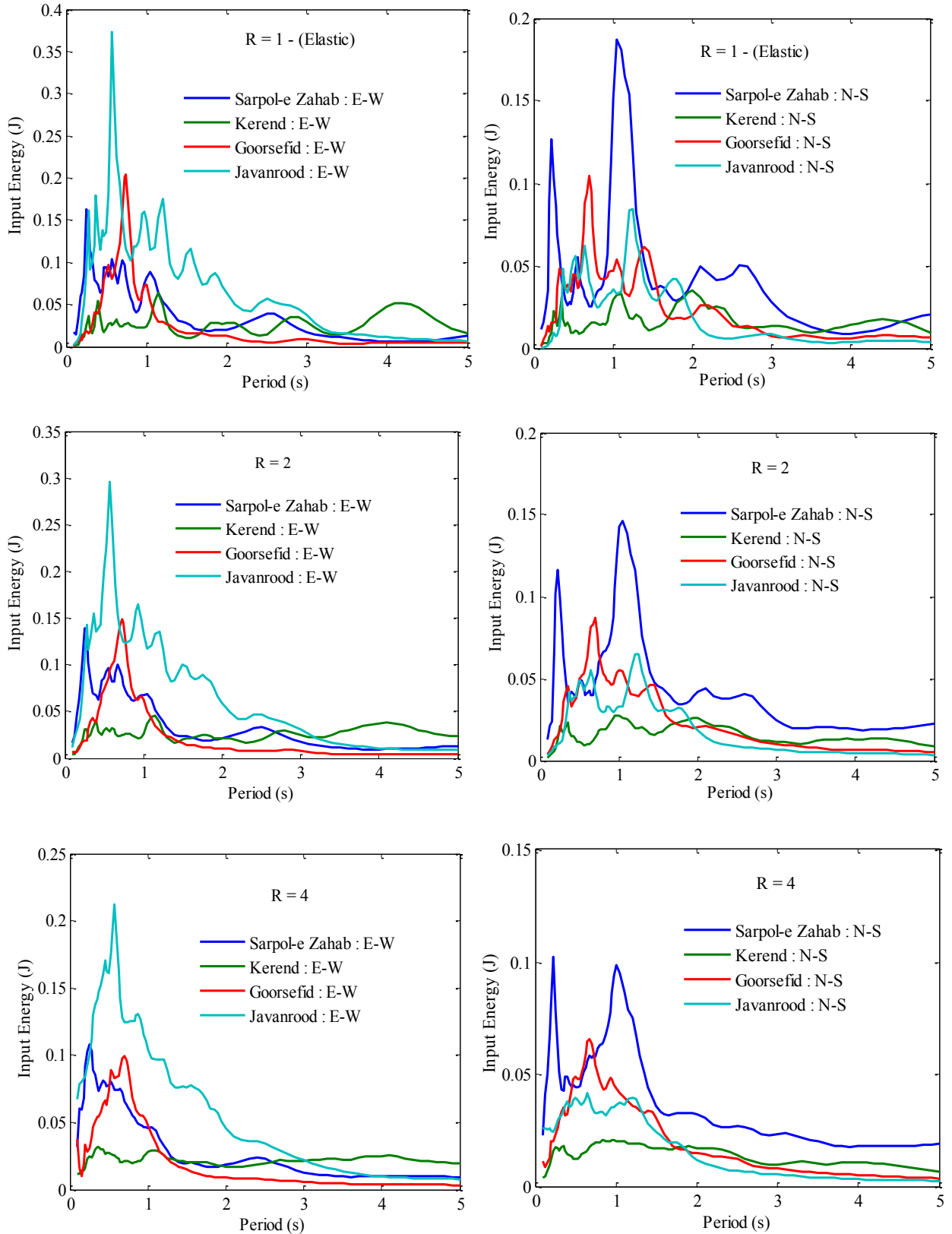
Fig. 13. Comparison of elastic and inelastic input energy spectra (R= 1,2 and 4) of selected records.

forces and displacements have been developed where the loading effect of the earthquake is interpreted in terms of input energy [29-32]. The energy balance equation for a

SDOF system can be written as [33]:
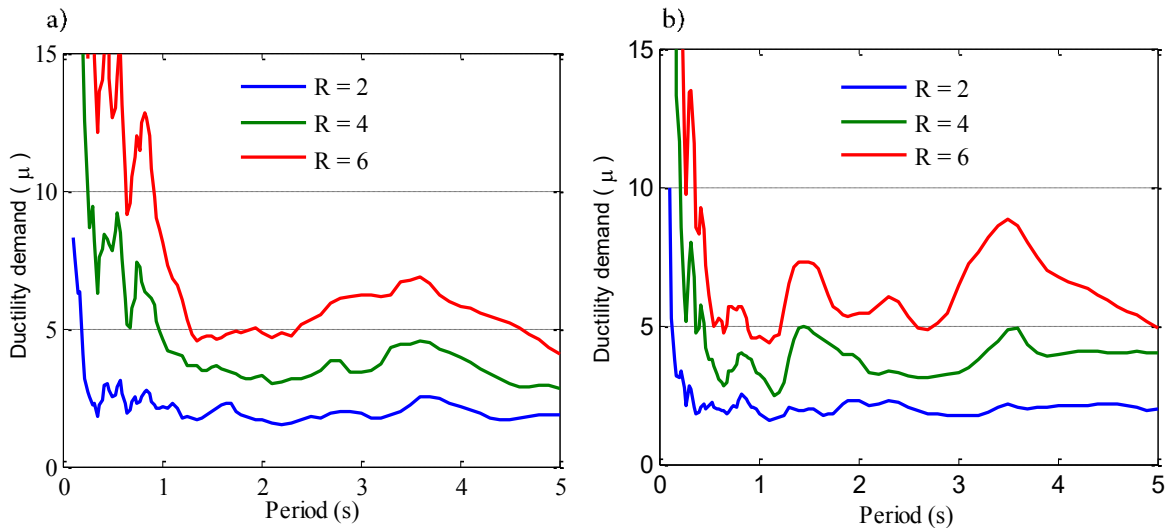
Fig. 14. Comparison of mean ductility demands computed from: a) E-W components, b) N-S components.

$$\int_0^t m\ddot{u}\dot{u}dt + \int_0^t c\dot{u}^2dt + \int_0^t f_s\dot{u}dt = \int_0^t m\ddot{u}_g\dot{u}dt \qquad (8)$$

The right-hand side of Eq. (8) expresses the total energy input (*EI*) that is imposed to the structure. Thus:

$$EI = -\int_0^t m\ddot{u}_g\dot{u}dt \qquad (9)$$

Where m is mass of the system; $\ddot{u}g$ is ground acceleration and $\dot{u}$ is the relative velocity of the system with respect to the ground. Elastic and inelastic input energy spectra for different components of selected records are compared in this par for inelastic SDOF systems with bilinear hysteretic behaviors and three strength reduction factor values (R = 1, 2, and 4)(Fig. 13). Based on Fig. 13, the E-W components have a larger input energy compared to the N-S components. Comparison of input energy of N-S components illustrates that the maximum input energy (E = 1.85 j) could be found at N-S component of Sarpol-e Zahab record with amplification in the period of vibration around 1.2 sec. Moreover, maximum input energy could be found at E-W component of Javanrood record.

7. DUCTILITY DEMAND SPECTRA

It is well known that structural damage is directly related to ductility demands [34] and therefore evaluation of ductility demand is very important for the structural performance under earthquake excitations. To consider the seismic demands of structures under the selected records, another parameter discussed herein is ductility demand. Ductility is defined as:

$$\mu = \frac{x_m}{x_y} \qquad (10)$$

Where x_m and x_y represent the maximum displacement and the yield displacement, respectively, of a nonlinear SDOF system. Fig. 14 shows mean ductility demands of inelastic SDOF systems with bilinear hysteretic behaviors computed from the E-W and N-S components of selected ground motions for three strength reduction factor values (R = 2, 4 and 6). It can obviously be observed that N-S components counterparts for structures with fundamental periods smaller than about 1.2s are smaller than mean ductility demands under E-W components.

8. SUMMARY AND CONCLUSIONS

In the current research, we investigated elastic and inelastic seismic demands computed from selected earthquake ground motions recorded during 12 November 2017 (Mw=7.3) Ezgeleh earthquake at various soil sites in the Kermanshah city. In this study, wavelet transform theory was used as a powerful tool for time-frequency analysis of selected ground motions. Results of wavelet analysis highlighted that energy of ground motions recorded at Sarpol-e Zahab station was concentrated in time and dominant period that caused heavy damage in buildings with the low fundamental period (i.e., 0.2-0.5 sec). Also, wavelet analysis shows that the type of strong long-period component present in the N-S component of the Sarpol-e Zahab record is caused by the directivity effect. Wavelet map of the E-W component of Javanrood record shows amplification in period range from 0.5 to 2 sec due to the significant soil softening.

Inter-story drift spectrum computed from the selected earthquake records showed that those from the E-W component generated greater mean inter-story drift demands than from the N-S direction. Particularly, it was identified that Sarpol-e Zahab and Goorsefid stations produced inter-story drift demands significantly larger than those at other recording stations. Inter-story drift spectra of N-S component of Sarpol-e Zahab station show a typical amplification in the period around 1.2 sec. This amplification could be associated

to presence of pulse caused by the directivity effect.

Results of nonlinear analysis highlighted that mean ductility (µ) demands of the E-W components are larger than the counterparts from the N-S components for structures with fundamental periods shorter than 1.2 sec.

In this investigation, the input energy spectra computed from bilinear SDOF systems subjected to selected earthquake records are significant for structures with elastic periods shorter than 1.5 sec. In this spectral region, the difference is related to the level of relative lateral strength of the system.

9. ACKNOWLEDGEMENTS

REFERENCES

[1] Preliminary report on 12th November 2017, magnitude 7.3 earthquake in Sarpol-e Zahab, Kermanshah Province, 5rd Edition, November 2017, International Institute of Earthquake Engineering and Seismology (IIEES), Tehran, Iran (in Persian).

[2] BHRC. last accessed February 2019 n.d, http://smd.bhrc.ac.ir/Portal/en/Search/ Waveforms.

[3] A preliminary report on school buildings performance during M 7.3 Ezgeleh, Iran earthquake of November 12, 2017

[4] L. Cohen, Time-frequency analysis, Prentice Hall PTR Englewood Cliffs, NJ, 1995.

[5] F. Auger, P. Flandrin, P. Gonçalvès, O. Lemoine, Time-frequency toolbox, CNRS France-Rice University, 46 (1996).

[6] B. Burke-Hubbard, The world according to wavelets: The story of a mathematical technique in the making, (1998).

[7] S. Yaghmaei-Sabegh, Time–frequency analysis of the 2012 double earthquakes records in North-West of Iran, Bulletin of earthquake engineering, 12(2) (2014) 585-606.

[8] S. Yaghmaei-Sabegh, J. Ruiz-García, Nonlinear response analysis of SDOF systems subjected to doublet earthquake ground motions: A case study on 2012 Varzaghan–Ahar events, Engineering Structures, 110 (2016) 281-292.

[9] M.R. KARAMI, B. Ghanbari, A. Akhaveissy, A new approach to identify active frequencies of dynamic ratcheting-inducing ground motion, (2017).

[10] Yazdani, T. Takada, Wavelet-Based Generation of Energy-and Spectrum-Compatible Earthquake Time Histories, Computer-Aided Civil and Infrastructure Engineering, 24(8) (2009) 623-630.

[11] Z. Zhou, H. Adeli, Time-frequency signal analysis of earthquake records using Mexican hat wavelets, Computer-Aided Civil and Infrastructure Engineering, 18(5) (2003) 379-389.

[12] P. Naga, M. Eatherton, Analyzing the effect of moving resonance on seismic response of structures using wavelet transforms, Earthquake engineering & structural dynamics, 43(5) (2014) 759-768.

[13] E. Smyrou, İ.E. Bal, P. Tasiopoulou, G. Gazetas, Wavelet analysis for relating soil amplification and liquefaction effects with seismic performance of precast structures, Earthquake Engineering & Structural Dynamics, 45(7) (2016) 1169-1183.

[14] S. Yaghmaei-Sabegh, Interpretations of ground motion records from the 2017 M w 7.3 Ezgeleh earthquake in Iran, Bulletin of Earthquake Engineering, 17(1) (2019) 55-71.

[15] H.B. Seed, S. HB, EVALUATION OF SOIL LIQUEFACTION EFFECTS ON LEVEL GROUND DURING EARTHQUAKES, (1976).

[16] Asakereh, M. Tajabadipour, Analysis of Local Site Effects on Seismic Ground Response under Various Earthquakes, AUT Journal of Civil Engineering, 2(2) (2018) 227-240.

[17] J.F. Perri, J.M. Pestana, Ground motion analysis with the use of the short-time-response-spectrum, Journal of Earthquake Engineering, 21(3) (2017) 384-410.

[18] M. Hadi, F. Behnamfar, S. Arman, A Shear-based Adaptive Pushover Procedure for Moment-resisting Frames, AUT Journal of Civil Engineering, 2(2) (2018) 183-194.

[19] D.A. Skolnik, J.W. Wallace, Critical assessment of interstory drift measurements, Journal of structural engineering, 136(12) (2010) 1574-1584.

[20] A.H. Shodja, F.R. Rofooei, Using a lumped mass, nonuniform stiffness beam model to obtain the interstory drift spectra, Journal of Structural Engineering, 140(5) (2014) 04013109.

[21] E. Miranda, S. Akkar, Generalized interstory drift spectrum, Journal of structural engineering, 132(6) (2006) 840-852.

[22] P. Csonka, Simplified analysis for the calculation of multistory frames subjected to wind load, Müszaki Tudományok Osztályának Közleményei, 35(1-3) (1965) 209-229.

[23] A.R. Khaloo, H. Khosravi, Multi-mode response of shear and flexural buildings to pulse-type ground motions in near-field earthquakes, Journal of Earthquake Engineering, 12(4) (2008) 616-630.

[24] D. Yang, J. Pan, G. Li, Interstory drift ratio of building structures subjected to near-fault ground motions based on generalized drift spectral analysis, Soil Dynamics and Earthquake Engineering, 30(11) (2010) 1182-1197.

[25] Alonso-Rodríguez, E. Miranda, Assessment of building behavior under near-fault pulse-like ground motions through simplified models, Soil Dynamics and Earthquake Engineering, 79 (2015) 47-58.

[26] B. Ghanbari, A.H. Akhaveissy, Effects of pulse-like ground motions parameters on inter-story drift spectra of multi-story buildings, International Journal of Structural Engineering, 8(1) (2017) 60-73.

[27] J. Ruiz-García, E. Miranda, Evaluation of seismic displacement demands from the September 19, 2017 Puebla-Morelos (Mw= 7.1) earthquake in Mexico City, Earthquake Engineering & Structural Dynamics, 47(13) (2018) 2726-2732.

[28] A.K. Chopra, Dynamics of structures, Pearson Education India, 2007.

[29] G.W. Housner, Limit design of structures to resist earthquakes, in: Proc. of 1st WCEE, 1956, pp. 5.1-5.13.

[30] Y. Chai, P. Fajfar, K. Romstad, Formulation of duration-dependent inelastic seismic design spectrum, Journal of Structural Engineering, 124(8) (1998) 913-921.

[31] Y. Chai, P. Fajfar, A procedure for estimating input energy spectra for seismic design, Journal of Earthquake Engineering, 4(04) (2000) 539-561.

[32] P. Quinde, E. Reinoso, A. Terán-Gilmore, Inelastic seismic energy spectra for soft soils: Application to Mexico City, Soil Dynamics and Earthquake Engineering, 89 (2016) 198-207.

[33] F.S. Alıcı, H. Sucuoğlu, Elastic and inelastic near-fault input energy spectra, Earthquake Spectra, 34(2) (2018) 611-637.